Correlations between reaction product yields as a tool for probing heavy-ion reaction scenarios

W. Gawlikowicz,[1,2] D. K. Agnihotri,[1] S. A. Baldwin,[1] W. U. Schröder,[1,*] J. Tõke,[1] R. J. Charity,[3] D. G. Sarantites,[3] L. G. Sobotka,[3] R. T. deSouza,[4] T. Barczyk,[5] K. Grotowski,[5] S. Micek,[5] R. Płaneta,[5] and Z. Sosin[5]

[1]*Departments of Chemistry and Physics, University of Rochester, Rochester, New York 14627, USA*

[2]*Heavy-Ion Laboratory, Warsaw University, PL-02-093 Warsaw, Poland*

[3]*Department of Chemistry, Washington University, St. Louis, Missouri 63130, USA*

[4]*Department of Chemistry, Indiana University, Bloomington, Indiana 47405, USA*

[5]*Institute of Physics, Jagellonian University, PL-30-059 Krakow, Poland*

(Received 29 May 2009; published 8 January 2010)

Experimental multidimensional joint distributions of neutrons and charged reaction products were analyzed for ^{136}Xe + ^{209}Bi reactions at $E/A = 28$, 40, and 62 MeV and were found to exhibit several different types of prominent correlation patterns. Some of these correlations have a simple explanation in terms of the system excitation energy and pose little challenge to most statistical decay theories. However, several other types of correlation patterns are difficult to reconcile with some, but not other, possible reaction scenarios. In this respect, correlations between the average atomic numbers of intermediate-mass fragments, on the one hand, and light particle multiplicities, on the other, are notable. This kind of multiparticle correlation provides a useful tool for probing reaction scenarios, which is different from the traditional approach of interpreting inclusive yields of individual reaction products.

DOI: 10.1103/PhysRevC.81.014604 PACS number(s): 25.70.Pq, 25.70.Mn

I. INTRODUCTION

Over the last 20 years or so, considerable effort has been made, both experimentally and theoretically, to explore heavy-ion reaction dynamics and to understand the production scenarios of various products. As a result of this effort, a consensus has emerged as to the general collision scenario prevailing at low bombarding energies and, perhaps, also in the lower part of the Fermi-energy domain. In this "consensus" domain, the projectile and target are believed to proceed in the manner of a dissipative collision, where they transiently form a revolving dinuclear complex and convert an ever-increasing (with time) portion of the kinetic energy of relative motion into intrinsic thermal and rotational energies. The phenomena of energy and angular momentum dissipation and mass transfer are thought to be effected mainly by means of stochastic nucleon exchange between projectilelike and targetlike constituents. Subsequently, the dinuclear complex reseparates under the combined action of Coulomb and centrifugal forces, and the projectilelike (PLF) and targetlike (TLF) fragments are set free to proceed on their individual Coulomb trajectories. Furthermore, the PLFs and TLFs are believed to emerge from the dissipative collision excited and thermally equilibrated and, accordingly, to decay statistically. Superimposed on this simple scenario, but not interfering with it to any significant extent, is pre-equilibrium emission of neutrons and light charged particles (LCPs), occurring mostly in early stages of the collision history. It is important to note that observations of individual product yields, and, specifically, of patterns in the yield distributions characteristic of the inferred consensus scenario, were instrumental in arriving at this consensus picture. For example, a notorious pattern is that seen in typical Wilczyński plots [1] of PLF yield as a function of PLF kinetic energy and deflection angle.

At higher bombarding energies, up to $E/A = 62$ MeV, the underlying general dissipative collision scenario still appears to be consistent with a variety of experimental observations made at energies close to the interaction barrier [2]. However, a consensus is still lacking as to the dominant production mechanisms of the observed light and intermediate-mass reaction products. To some extent, this is because of expectations of an increased role of two-body interactions and of increased pre-equilibrium emission, possibly including emission from the dynamically unstable interfragment "necklike" structure [3–5]. But more importantly, it is because of the observation of copious production of intermediate-mass fragments (IMFs), which exhibits certain aspects of statistical independence [6,7] but appears to be difficult to reconcile with classical scenarios of the statistical decay of an equilibrated nuclear system. A number of unconventional statistical approaches have been developed [8–10] to address the shortcomings of traditional models of statistical particle emission when applied to IMFs. On the contrary, several experimental studies [11–15] have concluded a dominantly nonequilibrium mode of IMF production.

The failure to reach a consensus at these higher energies may well point to inherent limitations of available data sets and/or of their analysis, which calls for additional, extended analysis schemes involving various correlations between the production patterns of different species, such as neutrons, LCPs, IMFs, PLFs, and TLFs.

With the potential probative value of such correlations in mind, a series of experiments was performed in which all of the many types of products were measured simultaneously, event by event. More specifically, in these experiments both neutrons and charged reaction products were measured with 4π angular coverage using the University of Rochester

*schroeder@chem.rochester.edu

SuperBall or RedBall neutron calorimeter/multiplicity meters in combination with one of the available 4π charged-product detector arrays (Michigan State University MiniBall, Washington University Dwarf Ball/Wall and MicroBall). Additionally, PLFs were measured at forward angles, also with a high geometrical efficiency resulting from their strong kinematic focusing.

The present study focuses on experimental data on ^{139}Xe + ^{209}Bi reactions at $E/A = 28$, 40, and 62 MeV and aims at evaluating the significance of three types of prominent correlation patterns observed in multidimensional joint distributions of neutrons—LCPs, IMFs, and PLFs—as a tool for probing the underlying reaction scenario and, by implication, the production mechanisms of these species. The correlations considered include those between the neutron and the charged-particle multiplicities, between the average size of IMFs and the joint neutron and LCP multiplicity, and between the average size of PLFs and the joint neutron and LCP multiplicity.

II. ESSENTIALS OF THE EXPERIMENTAL SETUP

The experiment was performed at the National Superconducting Cyclotron Laboratory of Michigan State University. Beams of ^{136}Xe ions from the K1200 cyclotron, with energies of $E/A = 28, 40$, and 62 MeV, were focused on a self-supporting 3.5-mg/cm^2-thick ^{209}Bi target placed in the operational center of the detector setup. The latter consisted of two 4π detector systems: the Washington University charged-particle detector array, Dwarf Ball/Wall [16], and one of the University of Rochester neutron calorimeter/multiplicity meters, SuperBall [17] or RedBall. Additionally, two position-sensitive silicon-detector telescopes were placed at forward angles, so as to cover an angular range encompassing the anticipated grazing angle ($\theta_{\text{Grazing}} = 4.48^\circ$, 3.90°, and 2.91° for 28, 40, and 62 MeV/nucleon reactions, respectively). The Dwarf array provided for reliable Z identification for atomic numbers up to $Z = 35$ and also for energy and emission angle measurement [18]. The SuperBall provided for high-efficiency, event-by-event measurement of neutron multiplicities and of summed kinetic energies of neutrons, in five angular bins. Because the mean detection efficiencies for the relatively weak components of high-energy pre-equilibrium neutrons and protons are much lower [17,19] than those for the less energetic, statistically emitted particles, the multiplicities measured for neutrons and LCPs reflect mainly the thermal excitation energies of the emitter nuclei.

The forward-angle telescopes provided for Z identification of PLFs, along with energy and angle measurement. They were also sensitive to IMFs. In all cases, the "minimum bias" trigger for data acquisition was the registration of one charged particle by any of the detectors. Although even elastic scattering of projectiles was measured in the experiments, a PLF coincidence was not required in the definition of the minimum bias trigger. Thus the experimental setup allowed almost-complete characterization of individual reaction events in terms of product identification, product yields, and corresponding kinematic parameters.

III. THEORETICAL MODELING OF VARIOUS REACTION SCENARIOS

The ultimate goal of modeling of any particular reaction scenario is to obtain model predictions for experimentally measured patterns in reaction product yields, so the latter can be used to verify the consistency of, or to falsify, the scenario under scrutiny. Given the complex nature of the processes leading from the heavy-ion collision to the detection of products, modeling is in practice always a multistep endeavor involving both a "fundamental" modeling of the physical phenomena of interest and a more technical modeling of the detection processes. Quite generally, the latter is free of hypotheses and includes modeling of the geometric and electronic acceptance (thresholds, dynamical ranges) of reaction products by the detector setup, but it may also include calculations of multiparticle Coulomb trajectories from the moment at which the particles are set free in the fundamental theoretical models to the moment when they reach their respective asymptotic trajectories.

In heavy-ion reactions at low and intermediate bombarding energies, the fundamental theoretical modeling itself is typically a two-step process, with the first step aiming to describe the collision dynamics and the second aiming to describe the decay of the primary reaction products. Generally, the outcome of such simulation calculations depends on assumptions made in both steps, which tends to obscure an interpretation of possible discrepancies between predictions and experimental observations. Therefore, predictions of patterns that are uniquely sensitive to one of the two steps but not the other are of special value.

In the present study, two theoretical codes were used alternately to model the dynamical, interaction stage of the collision, whereas two other codes were used alternately to model the subsequent statistical decay of the primary products emerging from the interaction stage with the dynamical model predictions for product mass and atomic numbers, excitation energies, and spins. Thus, the interaction stage was modeled using either the classical transport code CLAT [20], based on a stochastic nucleon exchange model (NEM) [21], or the quantum molecular dynamics (QMD) code CHIMERA [22], accounting in more detail for two-body interactions. The version of the CHIMERA code used [22] included isospin-dependent nuclear interactions, and calculations were performed for the time interval from 0 up to 300 fm/c assuming a soft equation of state (EOS; $K \approx 200$ MeV) with a symmetry energy strength coefficient corresponding to an ASY-STIFF EOS ($C = 31.4$ MeV) [23].

The statistical decay of the primary fragments predicted by the dynamical models of the interaction stage was then modeled using either the equilibrium-statistical, sequential decay code GEMINI [24] or the (pseudomicrocanonical) statistical multifragmentation code SMM [8].

Note that the physical scenario nominally implemented in the code CLAT may not be a very accurate representation of the interaction at higher bombarding energies. What matters in the present study, however, is that it provides a surprisingly good effective parametrization of the interaction, in particular, of the dissipation function. The code SMM, on the other hand,

as a matter of principle does not represent any realistic physical scenario that can be supported by generally accepted theories of nuclear matter. Therefore, this code is also viewed merely as providing a reasonably good effective parametrization of the statistical decay of excited nuclear systems.

A multiparticle Coulomb trajectory calculation routine [25] was applied to the end products predicted by the "standard" GEMINI code [24], making use of the (statistical) timing, spatial locations, decay axes, and relative energies of all (binary) decays along the de-excitation cascade. This kinematic "afterburner" allowed the calculation of energies and asymptotic emission angles of all reaction products.

The results of model calculations were subsequently passed through a routine calculating the response of the Dwarf Ball/Wall and SuperBall 4π detector systems to each and every reaction product predicted by the model calculations. The routine accounted for the geometric acceptance and the detection efficiency of all detectors for various particle species. The efficiency of the SuperBall was calculated using a version of the well-known code DENIS [26]. This procedure of converting "generic" theoretical predictions into custom predictions for a given detection setup is often called "filtering." The "filtered" model predictions can then be compared meaningfully to the experimental data.

IV. EXPERIMENTAL RESULTS AND ANALYSIS

In this section, three types of prominent correlations between the yields of four distinct classes of reaction products—neutrons, LCPs, IMFs, and PLFs—are discussed and analyzed in terms of various reaction scenarios, represented by pairs of theoretical models already discussed.

A. Neutron and light charged particle multiplicity correlation patterns

It is well known from the literature [27–29] that the joint multiplicity distributions of neutrons and LCPs can be used as measures of kinetic energy dissipation achieved in individual reaction events. This distribution for the $^{136}\mathrm{Xe} + {}^{209}\mathrm{Bi}$ reaction at $E/A = 40\,\mathrm{MeV}$ is shown in Fig. 1(a) in the form of a (logarithmic) contour plot, and the respective distributions expected for different interaction/decay scenarios are shown in Figs. 1(a)–1(d). As shown in Fig. 1(a), the experimental two-dimensional joint multiplicity distribution features a prominent intensity ridge with a crest line initially running parallel to the neutron multiplicity axis and then, at $m_n \approx 20$, turning away from this axis, to continue along a line running at an angle with respect to the coordinate axes. This behavior has a natural explanation in phase-space-based statistical decay models, which strongly favor neutron emission at low excitation energies, hence the section of ridge parallel to the m_n axis. At higher excitation energies, when the nuclear temperature becomes comparable to the height of the Coulomb barrier for the emission of LCPs, emission of the latter can successfully compete with neutron emission.

A somewhat less conspicuous feature of the joint neutron-LCP multiplicity distribution is the presence of a "pass" in the ridge at around $(m_{\mathrm{LCP}}, m_n) \approx (5, 28)$. Note that both terms, pass and ridge, refer to a hypersurface in the three-dimensional space spanned by particle multiplicities and by the number of events. Mathematically, the pass is a saddle point on this hypersurface. As the distance along the ridge from the origin of the plot represents the excitation energy in the system reasonably well [28], the presence and location of the pass are reflections of a particular mix of dissipative and conservative forces acting between the collision partners. More specifically, they are reflections of the form of dissipation function, that is, of the impact-parameter dependence of the dissipated energy. Hence, the location of the pass can possibly be used to validate effective interactions employed in collision codes, a task that is beyond the scope of the present study.

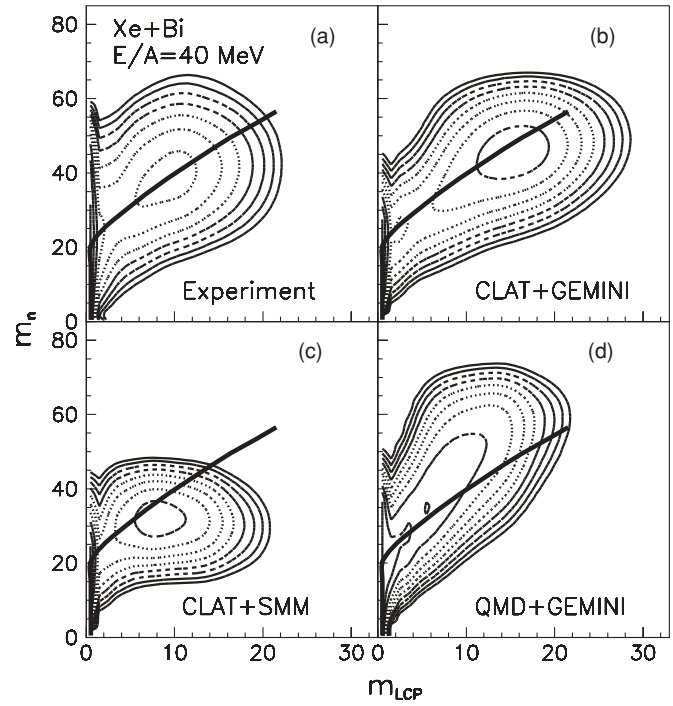

FIG. 1. Logarithmic (base 2) contour plots of experimental (a) and various model (b–d) joint distributions of the neutron (m_n) and light charged particle (m_{LCP}) for the $^{136}\mathrm{Xe} + {}^{209}\mathrm{Bi}$ reaction at $E/A = 40\,\mathrm{MeV}$.

The experimental crest line is shown in Figs. 1(a)–1(d), liberally extrapolated beyond the high-multiplicity peak of the ridge. Note that the ridge cannot be uniquely defined mathematically beyond that peak.

As shown in Fig. 1, all theoretical scenarios, represented here by combinations of model codes—CLAT + GEMINI (one-body interaction and sequential decay), CLAT + SMM (one-body interaction followed by decay of systems in "freeze-out" configurations), and QMD + GEMINI (one- and two-body dynamics followed by sequential decay of primary products)—tend to reproduce the general appearance of the joint multiplicity distribution. However, there are significant differences regarding the quality of the resemblance between the experimental plot, on the one hand, and various theoretical predictions, on the other hand.

It appears that the least complex calculations, based on the codes CLAT [20] and GEMINI [24], provide for the

best agreement with experimental observations, as far as the location of the crest line of the yield ridge and the location of the pass in the ridge are concerned. However, they still fail to reproduce the location of the peak at high particle multiplicities. In model calculations, the latter location depends on the "dissipation function," describing the way in which the degree of kinetic energy dissipation effected depends on the impact parameter. However, it is not clear whether the observed discrepancy between the actual and the model locations of the high-multiplicity peak is caused partially or wholly by a flawed modeling of the dissipation function by the code CLAT, with its particular implementation of the stochastic NEM. This is so because the CLAT + GEMINI combination entirely neglects the role of an effective intermediate-velocity source that emits particles, especially IMFs with average kinetic energies higher than the purely thermal energies characteristic of equilibrated PLF and TLF sources. Inclusion of pre-equilibrium emission and production of IMFs would result in shifting the peak in the theoretical (CLAT + GEMINI) yield ridge in Fig. 1(b) toward lower particle multiplicities, bringing it into better agreement with the experimental peak.

As shown in Fig. 1(c), a combination of the codes CLAT and SMM predicts a saturation in neutron multiplicity not observed experimentally, such that the model calculations "misplace" the crest line itself. There, not only the location of the high-multiplicity peak in the joint neutron and LCP multiplicity distribution, but also the location of the pass in the ridge disagree markedly with the experimental ones. Although these facts do not necessarily disqualify the SMM as a viable model, they point to specific model deficiencies in the description of relative neutron and LCP yields and should help in devising corrections to the model that remedy this deficiency.

As shown in Fig. 1(d), the QMD + GEMINI calculations largely fail to reproduce the "topography" of the yield ridge, such that they not only misplace the crest line, but also miss the pass in the ridge and the high-multiplicity peak altogether. Clearly, these model calculations overpredict the emission of neutrons compared with LCPs, which may indicate that the neutron yield is strongly affected by dynamical emission during the interaction stage of the collision. If so, this would be a deficiency that, apparently, cannot be remedied by simple *ad hoc* corrections to the QMD code CHIMERA [22]. Therefore, one may tentatively conclude that at $E/A = 40$ MeV, the collision dynamics is still largely governed by one-body dynamics and that the effects of direct nucleon-nucleon interactions are still too weak to justify the "universal" use of QMD logic to evaluate individual yields of all reaction products. However, the possibility that QMD provides a reasonably good description of the interaction stage for a limited range of impact parameters cannot be excluded.

In conclusion, we must note that the topography of the yield distribution as a function of neutron and LCP multiplicity, which features prominently a ridge, a pass, and a peak at high particle multiplicities, may serve not only as a primitive tool for validating theoretical models but also as a more nuanced tool for actually revising and upgrading these models.

B. Correlations between average fragment sizes and the joint multiplicity of neutrons and light charged particles

In recent years, prominent correlations between the average sizes of IMFs and the joint multiplicity of neutrons and protons have been discovered [2], which were also found to exhibit nonthermal scaling, such that they depend on the bombarding energy.

Such correlations are illustrated for three bombarding energies in Fig. 2, each in the form of a contour diagram of the average atomic number $\langle Z_{\rm IMF}\rangle$ of IMFs plotted versus the associated neutron and LCP multiplicity. No bias has been imposed on the distribution of IMFs admitted in these plots other than $3 \leqslant Z_{\rm IMF} \leqslant 16$. This segment of the product Z distribution is well separated from the domains of PLFs, their evaporation residues, and their fission fragments. As shown in Fig. 2, the average size of the IMFs produced is correlated prominently with the joint multiplicity of neutrons and LCPs, which reflects the dissipated and "thermalized" energy in heavy-ion collisions [27–29]. Hence, larger IMF sizes are associated with higher excitation energies. Interestingly, higher excitation energies also lead to higher multiplicities $M_{\rm IMF}$ of IMFs, which are mostly emitted [2] at excitation energies associated with the "central collision bump" in the joint

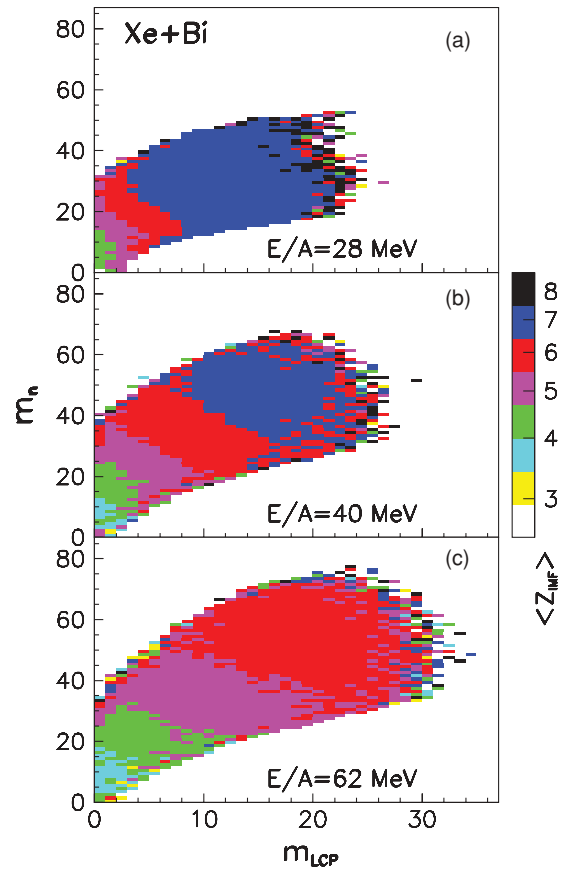

FIG. 2. (Color online) Logarithmic contour plot of the average atomic number of IMFs, $\langle Z_{\rm IMF}\rangle$, as a function of associated neutron and LCP multiplicity as observed in the ^{136}Xe + ^{209}Bi reaction at $E/A = 28$ MeV (a), $E/A = 40$ MeV (b), and $E/A = 62$ MeV (c). Here, $3 \leqslant Z_{\rm IMF} \leqslant 16$.

neutron/LCP multiplicity distribution mentioned previously. The clear "equisize" contour lines running almost perfectly parallel to each other appear to coincide with lines of constant excitation energy. They are a unique experimental manifestation of what is a trivial anticorrelation of neutron and LCP multiplicities in statistical decay models such as, for example, GEMINI [24]. Note that this kind of multiparticle correlation involves three independently measured quantities: the neutron and LCP multiplicities and the atomic numbers of IMFs.

Importantly, as is clear from comparison of Figs. 2(a)–2(c), the contour lines of equal $\langle Z_{\rm IMF}\rangle$ shift systematically toward higher neutron and LCP multiplicities as the bombarding energy increases, which suggests that they do not scale directly with the thermal excitation energy. This observation may then indicate that a significant portion of IMFs is produced in dynamical processes. Indeed, this kind of scaling of the average size of IMFs is consistent with scaling according to the size of the overlap region between projectile and target or, possibly, the size of the necklike structure formed transiently between the interacting PLF and TLF. This conclusion is based on the observation that, at higher bombarding energies, a comparatively smaller overlap region than at lower bombarding energies leads to the same given excitation energy, hence the shift of contour lines toward higher excitation energies but the same overlap. Although pre-equilibrium emission of neutrons and LCPs may also cause some shift of contour lines with bombarding energy, this shift is relatively small given the generally moderate multiplicity of pre-equilibrium particles. In fact, the presence of pre-equilibrium emission is expected to shift the lines in the direction opposite to that observed, as now the same thermal excitation energy will correspond to higher particle multiplicities.

Results of attempts to reproduce the observed correlations at $E/A = 40$ MeV by three reaction scenarios are illustrated in Fig. 3, along with the experimental distribution [Fig. 3(a)].

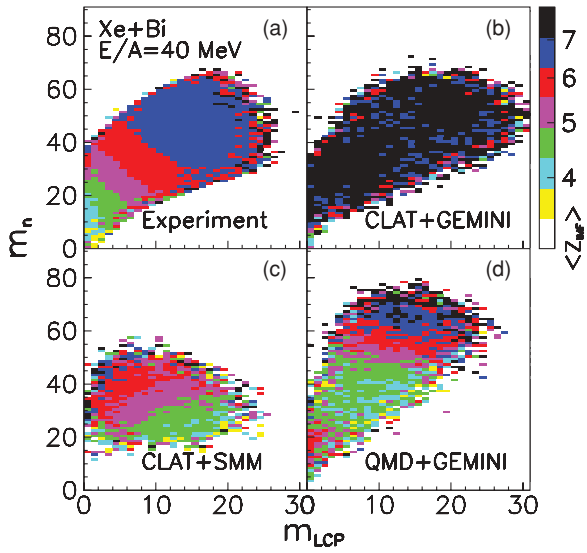

FIG. 3. (Color online) Logarithmic contour plots of average atomic numbers of IMFs, $\langle Z_{\rm IMF}\rangle$, as a function of associated neutron and LCP multiplicities, m_n and $m_{\rm LCP}$, as predicted by three sets of model calculations for $E/A = 40$ MeV (see text).

Model calculations always included the "experimental filter" accounting for the response of the detector setup. As shown in Fig. 3(b), the combined CLAT + GEMINI results resemble the data only insofar as the m_n-$m_{\rm LCP}$ correlation is concerned, and miss the size correlation pattern, consistent with the presence of the dynamical component in IMF yield as already discussed. This is also not surprising in view of the fact that very few IMFs are expected within the framework of these two models.

Figure 3(c) illustrates the failure of the statistical multifragmentation model SMM [8] to account for a prominent experimental correlation pattern. Although, based on the argument regarding the presence of a dynamical component in the IMF yield, one would not expect a particularly good agreement with experiment in this case, the correlations predicted for the CLAT + SMM scenario are, to a large extent, "orthogonal" to those actually observed. This may be taken to indicate a statistical multifragment breakup of an equilibrated system, such as would occur with SMM playing little, if any, role in IMF production in the bombarding energy range considered, and to suggest that IMF production occurs, perhaps, with no meaningful competition from particle decay channels.

Figure 3(d) illustrates predictions by the QMD code CHIMERA [22] complemented with the code GEMINI and the Coulomb trajectory "afterburner" [25]. Even though the CHIMERA scenario appears to be inconsistent with the correlation pattern seen in the joint distribution of neutron and LCP multiplicities, it may still be responsible for IMF production in a limited range of impact parameters. This is possible in view of the strong indication that IMFs, unlike neutrons and LCPs, are to a large extent produced in dominantly dynamical processes, expected to be well described by QMD-type codes. Indeed, as shown in Fig. 3(d), CHIMERA is capable of correctly rendering the trends observed experimentally, most notably, the increase in average IMF size with increasing neutron and LCP multiplicities. In this respect, it would be highly desirable to compare CHIMERA predictions with correlations observed experimentally for a range of bombarding energies.

C. Correlations between the size of projectilelike fragments and the joint multiplicity of neutrons and light charged particles

Figure 4 illustrates correlations between the average size of PLFs and the associated joint multiplicity of neutrons and LCPs, as observed at three bombarding energies: $E/A =$ 28 MeV [Fig. 4(a)], $E/A = 40$ MeV [Fig. 4(b)], and $E/A =$ 62 MeV [Fig. 4(c)]. As shown in Fig. 5, these correlations appear easy to understand within the prevailing scenario of a dissipative collision followed by statistical and sequential decay of primary PLFs and TLFs, as modeled by a two-step CLAT + GEMINI calculation. However, they can also be understood within the frameworks of the combined CLAT + SMM and the combined QMD + GEMINI scenarios. It appears, then, that this type of correlation is of lesser value as far as probing the more detailed interaction scenario is concerned. However, the fact that these correlations do not contradict conclusions reached earlier is in itself encouraging.

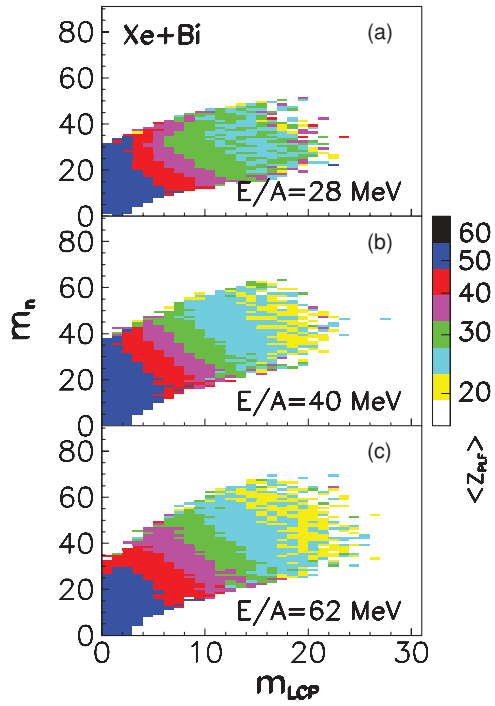

FIG. 4. (Color online) Logarithmic contour plot of average atomic numbers of the detected PLFs, $\langle Z_{\mathrm{PLF}} \rangle$, as a function of associated neutron and LCP multiplicities, as observed in $^{136}\mathrm{Xe} + ^{209}\mathrm{Bi}$ reactions at $E/A = 28$ MeV (a), $E/A = 40$ MeV (b), and $E/A = 62$ MeV (c).

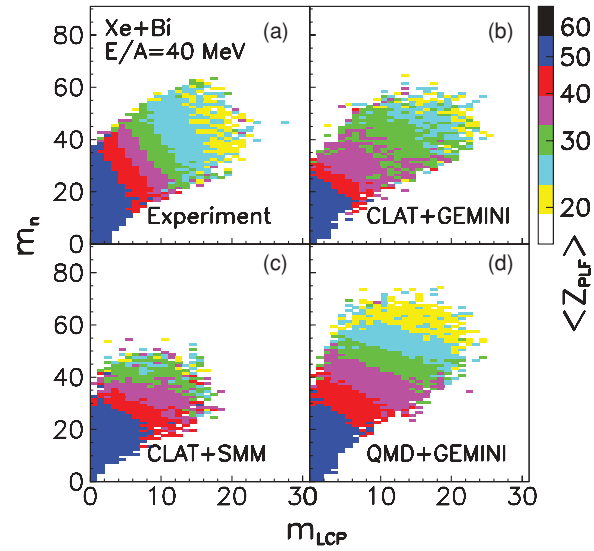

FIG. 5. (Color online) Logarithmic contour plot of average atomic numbers of PLFs, $\langle Z_{\mathrm{PLF}} \rangle$, as a function of associated neutron and LCP multiplicities, as predicted for the $^{136}\mathrm{Xe} + ^{209}\mathrm{Bi}$ reaction at $E/A = 40$ MeV by multistep simulation calculations using the codes CLAT + GEMINI (b), CLAT + SMM (c), and QMD + GEMINI (c).

V. SUMMARY

The present work has shown that certain prominent correlations observed between the yields of different reaction products can be used to probe the underlying collision and decay scenario and, hence, provide guidance in devising models of heavy-ion collision and decay of the excited primary products. Already the simple correlation pattern between the multiplicity of neutrons and that of LCPs tends to exclude dynamical QMD models as describing the overall collision scenario in the bombarding energy domain considered. It appears that, even at $E/A = 62$ MeV, the reaction dynamics is still largely dominated by one-body interactions, with a lesser propensity to pre-equilibrium release of particles and fragments than exhibited by a two-body interaction-dominated scenario.

Concerning IMF production, the relevance of a breakup state as modeled in an SMM-like freeze-out scenario appears to be strongly contradicted by the prominent experimental trends, and at this time there seems to be no obvious remedy for this deficiency of the SMM. The latter observation is perhaps related to the recently reported [30] inconsistency of SMM predictions with the IMF production observed in a spallation reaction, whereas the same data were well explained by GEMINI calculations. In that work [30], an intranuclear cascade code was used to simulate the interaction stage of the process.

In contrast, but in agreement with other recent work [11–14], the present study suggests that IMF production in heavy-ion reactions is dominated by dynamical processes resembling QMD-like scenarios. This conclusion is based largely on the bombarding-energy dependence of experimental correlations between the average size of IMFs and the joint neutron and LCP multiplicity reported, so far, in only one, very heavy-ion system.

ACKNOWLEDGMENTS

This work was supported by US Department of Energy Grant Nos. DE-FG02-88ER40414, DE-FG02-87ER-40316, and DE-FG02-88ER-40406, Polish Ministry of Science and Higher Education Grant No. N N202 035636, and M. Skłodowska-Curie Fund Grant No. MEN/DOE-97-318.

[1] J. Wilczyński, Phys. Lett. **B47**, 124 (1973).
[2] W. U. Schröder, in *Proceedings, International Workshop on Multifragmentation and Related Topics*, edited by R. Bougault *et al.* INFN Conf. Proc. Vol. 91 (2005), pp. 303–335.
[3] C. P. Montoya *et al.*, Phys. Rev. Lett. **73**, 3070 (1994).
[4] J. Tõke, B. Lott, S. P. Baldwin, B. M. Quednau, W. U. Schröder, L. G. Sobotka, J. Barreto, R. J. Charity, D. G. Sarantites, D. W. Stracener, and R. T. deSouza, Phys. Rev. Lett. **75**, 2920 (1995).
[5] S. Hudan, R. Alfaro, B. Davin, Y. Larochelle, H. Xu, L. Beaulieu, T. Lefort, R. Yanez, R. T. deSouza, R. J. Charity, L. G. Sobotka, T. X. Liu, X. D. Liu, W. G. Lynch, R. Shomin, W. P. Tan, M. B. Tsang, A. Vander Molen, A. Wagner, and H. F. Xi, Phys. Rev. C **71**, 054604 (2005).
[6] J. B. Elliott *et al.*, Phys. Rev. Lett. **88**, 042701 (2002).
[7] W. Skulski, J. Tõke, and W. U. Schröder, Phys. Rev. C **59**, 2130(R) (1999).

[8] J. Bondorf *et al.*, Phys. Rep. **257**, 133 (1995).
[9] D. H. E. Gross, Phys. Rep. **279**, 119 (1997).
[10] W. A. Friedman, Phys. Rev. Lett. **60**, 2125 (1988).
[11] F. Bocage *et al.*, Nucl. Phys. **A676**, 391 (2000).
[12] B. Davin *et al.*, Phys. Rev. C **65**, 064614 (2002).
[13] J. Colin *et al.*, Phys. Rev. C **67**, 064603 (2003).
[14] S. Piantelli *et al.*, Phys. Rev. Lett. **88**, 052701 (2002).
[15] E. de Filippo *et al.*, Phys. Rev. C **71**, 044602 (2005).
[16] D. W. Stracener *et al.*, Nucl. Instrum. Methods A **294**, 485 (1990).
[17] W. U. Schröder, Report DOE/ER/79048-1, 1995.
[18] W. Gawlikowicz, J. Tõke, and W. U. Schröder, Nucl. Instrum. Methods A **491**, 181 (2002).
[19] B. Djerroud, D. K. Agnihotri, S. P. Baldwin, W. Skulski, J. Tõke, W. U. Schröder, R. J. Charity, J. Dempsey, D. G. Sarantites, L. G. Sobotka, B. Lott, W. Loveland, and K. Aleklett, Phys. Rev. C **64**, 034603 (2001).
[20] W. U. Schröder *et al.*, Nucl. Sci. Res. Conf. Ser. **11**, 255 (1986).
[21] J. Randrup, Nucl. Phys. **A307**, 319 (1978); **A327**, 490 (1979); **A383**, 468 (1982).
[22] J. Łukasik *et al.*, Phys. Rev. C **55**, 1906 (1997).
[23] B. A. Li, L.-W. Chen, and C. M. Ko, Phys. Rep. **464**, 113 (2008).
[24] R. J. Charity *et al.*, Nucl. Phys. **A483**, 371 (1988).
[25] W. Gawlikowicz, Acta Phys. Pol. B **28**, 1687 (1997).
[26] J. Poitou and C. Signarbieux, Nucl. Instrum. Methods **114**, 113 (1974).
[27] U. Jahnke, G. Ingold, D. Hilscher, M. Lehmann, E. Schwinn, and P. Zank, Phys. Rev. Lett. **57**, 190 (1986).
[28] J. Tõke, D. K. Agnihotri, W. Skulski, and W. U. Schröder, Phys. Rev. C **63**, 024604 (2001).
[29] W. U. Schröder and J. R. Huizenga, in *Treatise on Heavy Ion Science, Vol. 2*, edited by D. A. Bromley (Plenum, New York, 1984), p. 113.
[30] E. Le Gentil *et al.*, Phys. Rev. Lett. **100**, 022701 (2008).